Hybrid fluid-structure interaction modelling of dynamic brittle fracture in pipeline steel transporting CO_2 streams

Reza H. Talemi[a,], Solomon Brown[b,c], Sergey Martynov[b], Haroun Mahgerefteh[b]

[a] *ArcelorMittal Global R&D Gent-OCAS NV, Pres. J.F. Kennedylaan 3, 9060 Zelzate, Belgium*
[b] *Department of Chemical Engineering, University College London, London, WC1E 7JE, UK*
[c] *Present address: Department of Chemical and Biological Engineering, University of Sheffield, S1 3JD, UK*

Abstract

Pressurised steel pipelines are considered for long-distance transportation of dense-phase CO_2 captured from fossil fuel power plants for its subsequent sequestration in a Carbon Capture and Storage (CCS) chain. The present study develops a hybrid fluid-structure methodology to model the dynamic brittle fracture of buried pressurised CO_2 pipeline. The proposed model couples the fluid dynamics and the fracture mechanics of the deforming pipeline exposed to internal and back-fill pressures. To simulate the state of the flow in the rupturing pipeline a compressible one-dimensional Computational Fluid Dynamics (CFD) model is applied, where the fluid properties are evaluated using rigorous thermodynamic model. In terms of the fracture model, an eXtended Finite Element Method (XFEM)-based cohesive segment technique is used to model the dynamic brittle fracture behaviour of pipeline steel.

Email address: Reza.HojjatiTalemi@ArcelorMittal.com (Reza H. Talemi)

Using the proposed model, a study is performed to evaluate the rate of brittle fracture propagation in a real-scale $48''$ diameter API X70 steel pipeline. The model was verified by comparing the obtained numerical results against available semi-empirical approaches from the literature. The simulated results are found to be in good correlation with the simulations using a simple semi-empirical model accounting for the fracture toughness, indicating the capability of the proposed approach to predict running brittle fracture in a CO_2 pipeline.
Keywords: CO_2 pipeline; Brittle fracture; Crack propagation; XFEM, CFD.

1. Introduction

The deployment of Carbon Capture and Storage (CCS) is the cornerstone of the drive to reduce CO_2 emissions (Metz et al., 2005). As part of the CCS chain, pressurised pipelines are widely recognised as the most practical and economical means of transporting the huge amounts of captured CO_2 from coal fired power plants for subsequent sequestration for onshore transportation. Typically, such pipelines may cover distances of several hundred kilometres at pressures above 100 bars. Transport of CO_2 in dense phase presents a high potential for auto-refrigeration due to depressurisation, either during operations or due to pipeline failure (Dooley et al., 2009). In general, dynamic brittle fractures are not of concern for modern gas transmission pipelines (Andrews et al., 2010). However, in the case of dense-phase CO_2, it has recently been suggested that the unusually high Joule-Thomson coefficient of CO_2 may induce low temperatures in the pipe upon the CO_2 fluid

expansion to atmospheric pressure (Mahgerefteh et al., 2006; Cosham et al., 2015). In the CO_2 expansion cloud temperatures as low as -78.5°C can be expected. In the case when a leak from the CO_2 pipeline produces such a cold stream enveloping the pipeline for a significantly long period of time, the pipe wall temperature can become significantly lower than the material nominal operating temperature, posing potential risk for brittle fracture initiation. In particular, for pipeline steels the ductile to brittle transition temperature (DBTT), at which the material ductility is significantly reduced, can be as high as -50°C (Billingham et al., 2003). As such, to ensure safe operation of CO_2 pipelines, the risk for brittle fracture and its consequences need to be correctly assessed.

In general, to prevent brittle fracture in pipelines, the pipe wall material is selected based on the brittle to ductile transition temperature, which should be lower than the minimal pipe wall temperature encountered during pipeline operation/decompression. However, using this criterion may not provide economically efficient solution, leading to over-design of the pipeline. Therefore, more accurate modelling of the pipeline decompression during a running fracture is required.

In the past the pipeline fracture propagation has been primarily studied for ductile fractures in the natural gas transmission pipelines (Maxey et al., 1972; O'Donoghue et al., 1997; Sugie et al., 1982; O'Donoghue et al., 1991; Greenshields et al., 2000; Higuchi et al., 2008; Yang et al., 2008; Nonn et al., 2013). Recently several authors have developed methodologies to couple pipeline outflow and crack propagation models (Greenshields et al., 2000; Aursand et al., 2014; Mahgerefteh et al., 2012; Nordhagen et al., 2012). These

methodologies are largely based on the Homogenous Equilibrium Mixture (HEM) model of pipe flow and utilise various models describing the pipe wall rupture, ranging from HLP-type models (Makino et al., 2001; Mahgerefteh et al., 2012) to FEM models accounting for ductile fracture of elasto-plastic material (Aursand et al., 2014). While the above studies have been focused on simulation of ductile fractures, modelling of the brittle mode of pipeline failure has not received as much attention yet. Practically this can be attributed to complex nature of brittle fracture propagation in steel pipes, which accurate description requires accounting for heat transfer and, importantly, the different mechanics of material failure in ductile and brittle modes. In particular, it has been shown that in contrast with the pipeline ductile fracture, the pipeline brittle rupture is characterized by a negligible amount of plastic deformations at the crack tip and is governed by the elastic stress in the pipe wall (Andrews et al., 2010). In some cases the brittle fracture advances at an axial velocity more than acoustic velocity in the fluid (Andrews et al., 2010).

To this end, the present study develops a hybrid fluid-structure modelling approach to simulate scenarios of pipeline failure involving brittle fracture propagation. The proposed model couples the fluid dynamics of the escaping fluid and the fracture mechanics of the deforming pipeline exposed to internal and back-fill pressures. To simulate the state of the fluid in the rupturing pipeline a one-dimensional compressible CFD model is developed accounting for the propagation of the crack tip into the pipe at a speed predicted by the material failure model. The latter, in its turn, is applied to calculate the crack propagation for the instantaneous state of stress (internal pressure) as predicted by the CFD model. In terms of fracture modelling, a novel

approach of the eXtended Finite Element Method (XFEM)-based cohesive segment technique is used to model the dynamic brittle fracture behaviour of pipeline steel. In this model the dynamic Stress Intensity Factor (SIF) and crack velocity are calculated at the crack tip at each crack propagation step.

The paper is organised as follows. Firstly, the hybrid fluid-structure interaction concept utilised to model the brittle fracture propagation is introduced in Section 2. This is followed by description of the pipeline decompression model (Section 3) and brittle fracture propagation model (Section 4). The results of the study are presented in Section 5 where the proposed fracture propagation model is verified and applied to a credible scenario of pipeline rupture. Section 6 states conclusions for the study.

2. Hybrid fluid-structure interaction modelling

The main objective of this study is to apply the hybrid FSI model to a hypothetical scenario of brittle fracture propagation in API X70 steel pipeline transporting CO_2 stream. While in reality, brittle mode crack propagation will occur only after the pipeline wall cooling by the released CO_2 stream to temperatures below Ductile to Brittle Transition Temperature (DBTT) and may be proceeded by ductile fracture, these phenomena significantly complicate the modelling. For this reason, in the present study, a conservative worst-case scenario assumption that the pipeline steel has embrittled as a result of cooling by CO_2 expansion process is made. This scenario would correspond to the case where a long-term leak preceding the brittle fracture propagation has produced a cold CO_2 cloud enveloping the pipeline, resulting in significant reduction in the pipe wall temperatures.

A pipeline running brittle fracture is a transient phenomenon, which involves dynamic coupling of the pipe wall fracture and the pipeline decompression. In particular, as a result of fracture propagation, the length of unfractured section of the pipeline decreases. In turn, as the pressure in the pipeline drops during the decompression, the driving force for the pipe wall deformations and fracture weakens, while speed of the fracture propagation may become reduced due to the change in the fluid compressibility caused by the flash-evaporation of the liquid. In order to model this coupled behaviour, the hybrid fluid-structure interaction concept is developed in the present study.

Figure 2 shows the corresponding hybrid fluid-structure interaction algorithm for the simulation of pipeline running brittle fracture. The developed hybrid modelling approach allows the quantitative prediction of the pipeline tendency to long running fractures in the form of the variation of crack length with crack velocity. At the beginning of simulation the bulk fluid pressure and the corresponding crack tip pressure are calculated by CFD model for a fixed small initial longitudinal crack opening along the major axis of the pipeline, formed for example, as a result of third party damage. The internal and back-fill pressures were applied by developing ABAQUS subroutine (DLOAD) which is used to define a non-uniform and distributed mechanical loads. Then, for an arbitrary small time increment, Δt, the pipeline rupture is simulated in ABAQUS, by defining a stationary XFEM crack, which gives the new position of the crack tip and the corresponding crack tip velocity. The crack velocity is calculated after extracting the SIF at the crack tip after each step of crack propagation. If the crack tip position reaches the end of

the pipe or the crack velocity turns to zero (the crack is arrested) the calculations are terminated. On the other hand, if the crack velocity is positive, it is passed to the CFD code where the position of the pipeline fracture (defined as the point where the pipe area expands by an arbitrary small value) is updated based on solution of an advection equation, and the amount of fluid released and the new crack tip pressure are calculated. For a new crack propagation step, the crack length is extended by an arbitrary small Δa. It is worth mentioning that, for simulating CO_2 pipe fracture, it was assumed that the crack propagation is dominated by opening fracture mode (Mode I). A Python script was written to repeat the above mentioned procedure up to the point at which the crack tip position reaches the end of the case study pipe.

The developed hybrid modelling concept assumes that running pipeline fracture can be modelled as an expansion in the pipe cross-section area from the initial cross-section area of the pipe A_0 to an arbitrary large area A_f. Figure 3(a) and (b) illustrate respectively the schematic representation of the pipeline section with a fracture along its length and the corresponding variation in the effective cross-sectional area of the pipeline in the proposed fracture dynamics model. In the one-dimensional flow model the pipe rupture is simulated as a continuous expansion in the pipe cross-sectional area, which happens over a short interval Δz. The fracture propagation is then modelled as motion of the expansion front at an instantaneous speed $\dot{a}$.

3. Pipeline decompression model

3.1. Flow model

In order to predict the state of the fluid in a pipeline during fracture propagation, the one-dimensional flow model is developed based on the decompression model describing oultflow from pipelines with stationary cracks (Mahgerefteh et al., 2006; Brown et al., 2015). This model uses the HEM assumption which implies thermal and dynamic equilibrium between saturated liquid and vapour phases, and accounts for a change in the flow area of the pipe. In the present study to account in the flow model for the effect of running fracture, the pipeline cross-sectional area is set as variable, changing from the initial area of the pipe to an arbitrary large value at the position of the crack tip.

The set of equations describing the HEM flow in a pipe includes the mass, momentum and energy conservation equations (Zucrow and Hoffman, 1976) augmented by an advection equation for the pipe cross-sectional area:

$$\frac{\partial A}{\partial t} + \dot{a}\frac{\partial A}{\partial z} = 0 \tag{1}$$

$$\frac{\partial A\rho}{\partial t} + \frac{\partial A\rho u}{\partial z} = 0 \tag{2}$$

$$\frac{\partial A\rho}{\partial t} + \frac{\partial A(\rho u^2 + P)}{\partial x} = P\frac{\partial A}{\partial z} - \frac{2f_w A\rho u^2}{D} \tag{3}$$

$$\frac{\partial AE}{\partial t} + \frac{\partial Au(E + P)}{\partial z} = P\frac{4Aq_w}{D} - \frac{2f_w A\rho u^3}{D} \tag{4}$$

where ρ, u and P are the mixture density, velocity and pressure respectively, which are functions of time, t, and space, z, D and A are respectively the local instantaneous pipeline diameter and cross-section area. q_w is the heat flux at the pipe wall, f_w is the Fanning friction factor calculated using Chen's correlation (Chen, 1979), and E is the total energy of the mixture per unit volume:

$$E = \rho\left(e + \frac{1}{2}u^2\right) \tag{5}$$

where e and ρ are the specific internal energy and density of the mixture respectively.

Equation 1 describes the advection of the pipeline expansion front at a speed $\dot{a}$, which is calculated using the developed brittle fracture model later. The shape of the expansion front is specified in the Lagrangian framework using a smooth function in a form:

$$A = f\left(A_f, \Delta z_f\right) \tag{6}$$

where A_f and Δz_f are the effective area of the expanded pipe and the smoothing distance, respectively.

3.2. Fluid properties

To calculate properties of the liquid and vapour phases and their equilibrium mixtures formed during the CO_2 pipeline decompression, the PC-SAFT equation of state is applied (Diamantonis et al., 2013). This equation of state has proved to provide superior accuracy in predicting the thermodynamic data for multi-component CO_2 mixtures covering the regions of

vapour-liquid equilibria (VLE) of relevance for CCS transportation pipelines (Diamantonis and Economou, 2011).

In the present study, for the sake of example, the pipeline fracture simulations are performed for CO_2 stream containing 3.5%(v/v) of N and 3.4%(v/v) of H_2S, which are typical impurities found in industrial-grade CO_2 captured using pre-combustion technology (Porter et al., 2015).

3.3. Numerical implementation

The governing partial differential equations, i.e. Equations 1-4, of the flow model can be solved subject to initial and boundary conditions for the flow at either end of the pipeline. At the closed end, located at z=0, the appropriate condition is u=0. At other end of the pipe, where the fracture propagation is initiated. i.e. z=l, where l is the total length of the pipeline, the fluid is exposed to the ambient pressure. Hence, a ghost cell (LeVeque, 2002) is utilized, in which $\partial\rho/\partial t$=0. The method of characteristics is used to apply the above boundary conditions in the numerical solution methodology as described by Thompson (1987). The numerical solution of the set of above mentioned quasi-linear hyperbolic equations describing flow in a variable cross-section are pipe is performed using the Finite-Volume Method as described by LeVeque (2002). Details of the implementation of this method were previously described by Brown et al. (2015), and for brevity are not included here.

4. Brittle fracture propagation model

There are many studies aimed to develop Finite Element (FE) models to describe the impact phenomena (Wu et al., 2013; Scheider et al., 2014; Nonn

et al., 2013). Wu et al. (2013) used the Gurson-Tvergaard-Needleman (GTN) model to simulate the fracture behaviour during DWTT. They analysed the equivalent stress, nucleation of voids and void size distribution using their FE Model. It was reported that the fracture propagates in a triangular shape at the crack tip, and inverse fracture occurs when the fracture propagated about 3/4 of sample width, they also found that in some of their simulations the transition during DWTT is from the brittle to the ductile and then again to the brittle zone. Scheider et al. (2014) have simulated ductile dynamic fracture propagation using a numerical approach with application of damage mechanics models and a cohesive zone method. Basically they used the GTN model to simulate the DWTT with pressed notch and pre-fatigued crack. They have derived numerical fracture resistance curves employed for the assessment of ductile fracture resistance. Nonn et al. (2013) modelled the ductile fracture behaviour of API X65Q pipeline steels subjected to DWTT using the GTN model. They have applied their model to describe and evaluate dynamic crack propagation in DWTT and pipe.

The majority of available studies in the literature, including the above reviewed ones, concentrated on numerical modelling of ductile behaviour of materials. There are limited studies that focus on brittle fracture of the DWTT or Charpy V-Notch (CVN) impact tests at low temperatures. For instance, Sainte Catherine et al. (2013) have developed the Beremin cleavage model to simulate CVN and sub-size CVN impact tests at low temperature. More recently, Talemi et al. (2016) have implemented a novel approach of the XFEM-based cohesive segment technique to simulate dynamic brittle fracture of pipeline steel subjected to CVN loading conditions.

In this study to simulate the crack propagation under dynamic mode, i.e. time dependent, two different modelling approaches was used. In the first step, crack propagation of DWTT was simulated under dynamic/Implicit mode in ABAQUS. In this step crack propagation was modelled using a moving crack. The ultimate goal of this simulation was to find the relationship between crack propagation speed and dynamic stress intensity factor at crack tip. In the second step, for fluid/structure interaction model, simulating the stationary crack was used to model the crack propagation in a pipe case study. The main difference between two approaches is that for the moving crack the time steps were calculated using dynamic/implicit solver in ABAQUS and for stationary crack, the time steps were calculated using the external CFD code based on extracted stress intensity factor at crack tip, from ABAQUS model, which is depicted in Figure 2.

4.1. Material and experiment

In this research an API X70 grade pipeline steel was used. The mechanical properties of the pipe were measured using round tensile bars with a diameter of 8 mm. To machine the tensile samples, a test plate was taken from the original pipe. All tests were carried out at different temperatures ranging from room temperature to -100°C under a low displacement rate of 0.036 mm/s. These data were subsequently used to determine the nominal and true stress-strain properties of the X70 steel grade. The Young's Modulus and yield stress measured at -100°C are E= 210GPa and σ_y= 760MPa, respectively.

In this study, in order to validate and calibrate the developed dynamic brittle fracture model, experimental data from a lab-scale Drop Weight Tear

Test (DWTT) at -100°C was used which were preformed according to ASTM E436. DWTT is a material characterisation test aimed at measuring the material's capability to arrest a running brittle fracture in pipelines. In a DWTT, the test specimen is a rectangular plate with a length of 305mm, a width of 76mm and of the full material thickness (up to at least 19mm). The specimen has a shallow pressed notch and is subjected to three-point bending impact loading, as shown in Figure 1. The standards specify a 5mm deep notch made by a sharp indenter with an inclined angle of 45°, resulting in a tip radius that is, in general, between 0.0127 to 0.0254mm.

4.2. XFEM-based cohesive segment approach

In general in case of local damage models for large scale simulations the mesh size at the crack tip and along the crack propagation path is an important parameter. However, in this study the mesh sensitivity has been decreased by using the XFEM formulation. Nevertheless, the density of the mesh in the vicinity of the critical zones should be appropriately refined as depicted in Figure 2.

One of the approaches within the framework of XFEM is based on traction-separation cohesive behaviour. This approach is used to simulate crack initiation and propagation. This is a very general interaction modelling capability, which can be used for modelling brittle or ductile fracture. The XFEM-based cohesive segments method can be used to simulate crack initiation and propagation along an arbitrary, solution-dependent path in the bulk material, since the crack propagation is not tied to the element boundaries in a mesh. In this case the near-tip asymptotic singularity is not needed, and only the displacement jump across a cracked element is considered. Therefore, the

crack has to propagate across an entire element at a time to avoid the need to model the stress singularity. In this study XFEM-based cohesive segment approach was used to model dynamic brittle fracture of CO_2 pipeline steel. To this end in this section the basic principles of both XFEM and Cohesive segment approaches are briefly reviewed.

XFEM principles

The XFEM approach was first introduced by Belytschko and Black (1999). It is an extension of the conventional finite element method based on the concept of partition of unity, which allows local enrichment functions to be easily incorporated into a finite element approximation. Crack modelling based on XFEM allows simulating both stationary and moving cracks. The method is useful for the approximation of solutions with pronounced non-smooth characteristics in small parts of the computational domain, for example near discontinuities and singularities. In these cases, standard numerical methods such as the conventional finite element method often exhibit poor accuracy. XFEM offers significant advantages by enabling optimal convergence rates for these applications. Simulation of propagating cracks with XFEM does not require initial crack and crack path definitions to conform to the structural mesh. The crack path can be solution dependent i.e., it is obtained as part of the solution, and the cracks are allowed to propagate through elements.

For the purpose of fracture analysis, the enrichment functions typically consist of the near-tip asymptotic functions that capture the singularity around the crack tip and a discontinuous function that represents the jump in displacement across the crack surfaces. The approximation for a displace-

ment vector function u with the partition of unity enrichment is

$$u^h(x) = \sum_{i=1}^{n} N_i(x) \left[u_i + H(x)a_i + \sum_{\alpha=1}^{4} F_\alpha(x) b_i^\alpha \right] \tag{7}$$

where $N_i(x)$ are the usual nodal shape functions; the first term on the right-hand side of the above equation, u_i, is the usual nodal displacement vector associated with the continuous part of the finite element solution; the second term is the product of the nodal enriched degree of freedom vector, a_i, and the associated discontinuous jump function $H(x)$ across the crack surfaces; and the third term is the product of the nodal enriched degree of freedom vector, b_i^α, and the associated elastic asymptotic crack-tip functions, $F_\alpha(x)$. The first term on the right-hand side is applicable to all the nodes in the model; the second term is valid for nodes whose shape function support is cut by the crack interior; and the third term is used only for nodes whose shape function support is cut by the crack tip. The discontinuous jump function across the crack surfaces, $H(x)$, is equal to +1 for $(x - x^*)n \leq 0$ and -1 otherwise, where x is a sample (Gauss) point, x^* is the point on the crack closest to x, and n is the unit outward normal to the crack at x^*. The asymptotic crack tip functions in an isotropic elastic material, $F_\alpha(x)$, are given by

$$\{F_\alpha(r,\theta)\}_{\alpha=1}^{4} = \left\{ \sqrt{r}\sin\left(\frac{\theta}{2}\right), \sqrt{r}\cos\left(\frac{\theta}{2}\right), \sqrt{r}\sin\left(\frac{\theta}{2}\right)\sin\theta, \ \sqrt{r}\cos\left(\frac{\theta}{2}\right)\sin\theta \right\} \tag{8}$$

where (r, θ) is a polar coordinate system with its origin at the crack tip and θ= 0 is tangent to the crack at the tip. These functions span the asymptotic crack-tip function of elasto-statics, $\sqrt{r}\sin(\theta/2)$ and take into account

the discontinuity across the crack face. Accurately modelling the crack-tip singularity requires constantly keeping track of where the crack propagates and is cumbersome because the degree of crack singularity depends on the location of the crack in a non-isotropic material. Therefore, the asymptotic singularity functions can only be used when modelling stationary cracks.

Cohesive segment principles

One of the approaches, within the framework of XFEM, that can be used to model a propagating crack is based on traction-separation cohesive behaviour. This approach is used to simulate crack initiation and propagation. This is a very general interaction modelling capability, which can be used for modelling brittle or ductile fracture. The XFEM-based cohesive segments method can be used to simulate crack initiation and propagation along an arbitrary, solution-dependent path in the bulk material, since the crack propagation is not tied to the element boundaries in a mesh. In this case the near-tip asymptotic singularity, $F_\alpha(x)$, is not needed, and only the displacement jump across a cracked element is considered. Therefore, the crack has to propagate across an entire element at a time to avoid the need to model the stress singularity. To this end, phantom nodes, which are superposed on the original real nodes, are introduced to represent the discontinuity of the cracked elements. When the element is undamaged, each phantom node is completely constrained to its corresponding real node. When the element is cut through by a crack, onset of damage initiation, the cracked element splits into two parts. Each part is formed by a combination of some real and phantom nodes depending on the orientation of the crack. Each phantom node and its corresponding real node are no longer tied together and can

move apart (Talemi et al., 2016).

The formulae and laws that govern the behaviour of XFEM-based cohesive segments for a crack propagation analysis are very similar to those used for cohesive elements with traction-separation constitutive behaviour. The similarities extend to the linear elastic traction-separation model, damage initiation criteria, and damage evolution laws. Damage modelling allows degradation and eventual failure of an enriched element. The failure mechanism consists of two portions: a damage initiation criterion and a damage evolution law. The initial response is assumed to be linear; however, once a damage initiation criterion is met, damage can occur according to a user-defined damage evolution law. Damage of the traction-separation response for cohesive behaviour in an enriched element is defined within the same general framework used for conventional materials. However, it is not necessary to specify the undamaged traction-separation behaviour in an enriched element.

Damage initiation refers to the beginning of degradation of the cohesive response at an enriched element. The process of degradation begins when the stresses or strains satisfy specified damage initiation criteria. In this study the maximum principal stress criterion was used in order to model crack initiation. The maximum principal stress criterion can be represented as

$$f = \left\{ \frac{\langle \sigma_{max} \rangle}{T_{max}} \right\} \tag{9}$$

where, T_{max} represents the maximum allowable principal stress. The symbol $\langle \sigma_{max} \rangle$ represents the Macaulay bracket with the usual interpretation (i.e., $\langle \sigma_{max} \rangle = 0$ if $\sigma_{max} < 0$ and $\langle \sigma_{max} \rangle = \sigma_{max}$ if $\sigma_{max} \geq 0$). The Macaulay brack-

ets are used to signify that a purely compressive stress state does not initiate damage. Damage is assumed to initiate when the maximum principal stress ratio (as defined in the expression above) reaches a value of one. Afterwards an additional crack is introduced or the crack length of an existing crack is extended after equilibrium increment when the fracture criterion, f, reaches the value 1 within a given tolerance. If $f \geq 1 + f_{tol}$ the time increment is cut back such that the crack initiation criterion is satisfied. In this study the value of f_{tol} was specified as 0.05.

The damage evolution law describes the rate at which the cohesive stiffness is degraded once the corresponding initiation criterion is reached. A scalar damage variable, D, represents the averaged overall damage at the intersection between the crack surfaces and the edges of cracked elements. It initially has a value of 0. If damage evolution is modelled, D monotonically evolves from 0 to 1 upon further loading after the initiation of damage. The normal and shear stress components are affected by the damage according to

$$t_n = \begin{cases} (1-D)T_n, & \text{if } T_n \geq 0 \\ T_n, & \text{otherwise} \end{cases} \tag{10}$$

$$t_s = (1-D)T_s \tag{11}$$

$$t_t = (1-D)T_t \tag{12}$$

where T_n, T_s and T_t are the normal and shear stress components predicted by the elastic traction separation behaviour for the current separations without damage. To describe the evolution of damage under a combination of

normal and shear separations across the interface, an effective separation is defined as

$$\delta_{max} = \sqrt{\delta_n^2 + \delta_s + \delta_t} \tag{13}$$

Concerning the damage variable D, an exponential model has been adopted to describe its evolution. In particular, according to such a model, the following relation holds

$$D = \int_0^{\delta_{max}} \frac{T_{max}}{\Gamma} d\delta \tag{14}$$

in which, Γ represents the cohesive energy, while δ_{max} is the effective displacement at complete failure. In terms of crack propagation direction, whenever the crack initiation criterion (maximum principal stress criterion) is met, the newly introduced crack is defined to be perpendicular to the maximum principal stress direction.

4.3. Finite Element Modelling

Two brittle fracture modelling approaches are used in this investigation, namely stationary and moving crack methodologies. The stationary crack modelling approach was used to model running brittle fracture in the pipe, as shown in Figure 2, and the propagating crack modelling approach was used to simulate the lab-scale Drop Weight Tear Test (DWTT) of the X70 pipeline steel at -100°C. To this end, to calculate the dynamic SIF at the crack tip during running brittle fracture propagation the DWTT configuration was modelled using ABAQUS software. The model consists of four parts, namely a hammer, two anvils and the DWTT specimen which can be

meshed independently. Figure 4 illustrates the finite element mesh of the specimen and an assembled view of the model.

A two-dimensional, 4-node (bilinear), plane strain quadrilateral, reduced integration element (CPE4R) was used in order to model the test configuration. A fixed rigid contour line represents the anvils and the hammer. The specimen is put on two rigid anvils and the hammer impacts the specimen under three point bending loading conditions. A mesh size of 0.5mm $\times$ 0.5mm was considered at the potential crack propagation regions and increased gradually far from the area of interest. Moreover, to correctly capture the multiaxial stress gradient at the notch tip the mesh size was decreased down to 0.05mm in this region. Contact was defined between the hammer and the specimen, as well as between the specimen and the anvils using a Coulomb friction law with a friction coefficient of 0.1. The contact between the hammer and the specimen along with the anvils and the specimen was defined using the master-slave algorithm. The surfaces of hammer and anvils were defined as slave surface and the surface of the specimen was defined as the master surface. The loading was modelled by prescribing the initial velocity of the hammer. The anvils were defined to remain fixed whereas the impact hammer could only move vertically. The impact hammer had an initial velocity of 6.5m/s and a mass of 985kg. In general explicit codes are used to capture the complicated system response as a function of time. Currently, the ABAQUS Dynamic/Explicit solver does not support the use of XFEM. However, it has been shown in the author's previous studies that the Dynamic/Implicit solver can be used to overcome this issue (Talemi et al., 2016; Talemi, 2016).

4.4. Material parameters

An experimental true stress-strain curve of API X70 at -100°C was used to simulate the material behaviour of the DWTT specimen. It is worth mentioning that in this study strain rate was not considered directly in the calculations of stress and strain fields. However, the strain rate does not have an influence on the cohesive stress value in the case of brittle fracture. The only part which is affected by strain rate is the cohesive energy (fracture energy). In this study the cohesive energy was calibrated using the data obtained from a dynamic impact test (DWTT). Therefore, the elastic-plastic material behaviour with isotropic hardening was defined. The enrichment area was chosen inside the area of interest for crack propagation which was the mesh refinement region.

Damage modelling allows simulation of crack initiation and eventual failure of the enriched area in the solution domain. The initial response is linear, while the failure mechanism consists of a damage initiation criterion and a damage propagation law. Damage initiation was defined based on the cohesive stress of T_{max}=1.4σ_y. The cohesive stress was determined by studying the damage process at the micro-scale using the so-called unit cell method as suggested by Scheider (2009). At the notch tip, the stress triaxiality varies with the increase of impact loading. For the cohesive zone model, it results in a change of the cohesive stress which depends on the stress triaxiality. In this study, the maximum value of the stress triaxiality at the notch tip was used for evaluating the cohesive stress in the unit cell method. Using the unit cell method, the maximum load carrying capacity can be captured during the damage initiation process under the given stress triaxiality, and the value of

the maximum load carrying capacity is equal to the cohesive stress. After obtaining the fracture toughness value using the Charpy V-Notch (CVN) impact test, the characteristic strength was obtained by varying the maximum stress in the traction-separation law, while maintaining the toughness at a constant value (Li et al., 2005). This means that the damage initiation parameter was calibrated, until the best agreement was achieved between the experimental and numerical load displacement curves.

When the damage initiation criterion is met, the damage propagation law starts to take place. In this study, the damage evolution was defined in terms of fracture energy (per unit area). Therefore, the fracture energy (Γ) was used for the damage evolution criteria. The cohesive energy was estimated using the relationship

$$\Gamma = G_{IC} = \frac{K_{IC}^2}{E/(1-\nu^2)} \tag{15}$$

where G_{IC} is the fracture energy, K_{IC} is the fracture toughness, E is the Young's modulus and ν is the Poisson ratio. The value for the fracture toughness was estimated from CVN energy. G_{IC} becomes the critical value of the rate of release in strain energy for the material which leads to damage evolution and possibly fracture of the specimen. The relationship between stress intensity and energy release rate is significant because it means that the GIC condition is a necessary and sufficient criterion for crack propagation since it embodies both the stress and energy balance criteria. Barsom and Rolfe (1970) suggested the correlation between CVN energy (J_{CVN}) and fracture toughness for the lower shelf of the DBTT curve, which is known as the Barsom-Rolfe correlation. They have examined the applicability of

various regression models in order to monitor the empirical relationship of fracture toughness with other mechanical properties such as KCV. They have found that for J_{CVN} and yield stress in ranges of 4-82J and 270-1700MPa respectively, the following practical equation can be derived

$$K_{IC} = 6.76[J_{CVN}]^{0.75} \tag{16}$$

In this study the mixed-mode behaviour was chosen and the fracture energies for those modes were introduced into XFEM. The fracture toughness values were selected as 25MPa$\times m^{0.5}$ for both Mode I fracture, opening mode (a tensile stress normal to the plane of the crack), and Mode II fracture, sliding mode (a shear stress acting parallel to the plane of the crack and perpendicular to the crack front). The same values for cohesive stress and energy have been applied successfully to simulate CVN impact test in the authors previous work (Talemi et al., 2016).

4.5. Dynamic stress intensity factor calculation

The dynamic SIF (K_{ID}) can be determined using various empirical approaches. Nishioka and Atluri (1982) have introduced an optimum technique for determining the dynamic SIF through the measurement of the Crack Mouth Opening Distance (δ_{CMOD}), applying the well-known relationship used in static conditions. Following the same proposed approach, the dynamic SIF was calculated from the FE results as:

$$K_{ID} = \frac{E\delta_{CMOD}}{\beta\sqrt{a\alpha}} \frac{C_1(\alpha)}{C_2(\alpha)} \tag{17}$$

where a is the crack length, β is the span-to-width ratio ($\beta = S/W$, shown

in Figure 4), α is the crack-to-width ratio ($\alpha = a/W$), and $C_1(\alpha)$ and $C_2(\alpha)$ are non-dimensional functions depending on α, values for both functions can be found in (Guinea et al., 1998). For the geometry considered in the present work these functions can be written as:

$$C_1(\alpha) = \frac{\sqrt{\alpha}}{(1-\alpha)^{1.5}(1+3\alpha)}(1.9 + 0.41\alpha + 0.51\alpha^2 - 0.17\alpha^3) \tag{18}$$

$$C_2(\alpha) = 0.76 - 2.28\alpha + 3.87\alpha^2 - 2.04\alpha^3 + \frac{0.66}{(1-\alpha)^2} \tag{19}$$

It is worth mentioning that in terms of modelling stationary cracks, the SIF was calculated by means of the path independent interaction integral. The interaction integral method is a technique to evaluate the mixed mode SIFs based on the J-Integral (Corten, 1980).The near-crack-tip stress field for a homogeneous, isotropic linear elastic material is given by

$$\sigma_{\theta\theta} = \frac{1}{\sqrt{2\pi r}} \cos\frac{\theta}{2}\left[K_I \cos^2\frac{\theta}{2} - \frac{3}{2}K_{II}\sin\theta\right] \tag{20}$$

$$\tau_{r\theta} = \frac{1}{2\sqrt{2\pi r}} \cos\frac{\theta}{2}\left[K_I \sin\theta + K_{II}(3\cos\theta - 1)\right] \tag{21}$$

where r and θ are polar coordinates centred at the crack tip in a plane orthogonal to the crack front. The constants of the stress field K_I and K_{II} represent the SIFs for the corresponding modes I and II, respectively, which can be obtained using interaction integral approach. This method was first proposed by Sih et al. (1965). They proposed based on this concept that the boundary value problem can be satisfied by superimposing auxiliary fields onto the actual fields. The auxiliary fields are arbitrarily chosen and are imposed in order to find a relationship between the mixed mode stress intensity

factors and the interaction integrals. The contour J integral in this method can be defined as:

$$J = J^{aux} + J^{act} + M \tag{22}$$

where J^{act} act and J^{aux} are associated with the actual and auxiliary states, respectively. M is defined as,

$$M = \oint_{\Omega} \left[\sigma_{ij}^{(act)} \frac{\partial u_i^{(aux)}}{\partial x_1} + \sigma_{ij}^{(aux)} \frac{\partial u_i^{(act)}}{\partial x_1} - W^{(M)} \delta_{ij} \right] \frac{\partial q}{\partial x_j} d\Omega \tag{23}$$

where

$$W^M = \frac{1}{2} \left(\sigma_{ij}^{(act)} \epsilon_{ij}^{aux} + \sigma_{ij}^{(aux)} \epsilon_{ij}^{act} \right) \tag{24}$$

where σ_{ij} are the stress tensor, u_i are the displacements, δ_{ij} is the Kronecker's delta and q is an arbitrary continuous function which must vanish at the outer boundary of the problem domain and must take the value 1 at the crack tip. The auxiliary fields are chosen to be the asymptotic crack tip fields for pure mode I or pure mode II to compute K_I and K_{II} respectively. The following equation defines the relationship of the J integral and K_I and K_{II},

$$M = \frac{2}{E'} \left(K_I K_I^{aux} + K_{II} K_{II}^{aux} \right) \tag{25}$$

where $E' = E/(1-\nu^2)$ and by putting K_I^{aux}=1 and K_{II}^{aux}=0, the mode I stress intensity factor can be obtained. K_{II} is obtained by setting K_I^{aux}=0

and K_{II}^{aux}=1, which can be written as:

$$K_I = \frac{E^{'}}{2} I^{(1,K_I^{aux})}; K_{II} = \frac{E^{'}}{2} I^{(1,K_{II}^{aux})} \tag{26}$$

Moreover, the direction of crack propagation can be obtained by implementing maximum tangential stress criterion using either the condition $\partial\sigma_{\theta\theta}/\partial\theta = 0$ or $\tau_{r\theta} = 0$; i.e.,

$$\theta_p = \cos^{-1}\left(\frac{3K_{II}^2 + \sqrt{K_I^4 + 8K_I^2K_{II}^2}}{K_I^2 + 9K_{II}^2}\right) \tag{27}$$

where the crack propagation angle θ_p is measured with respect to the crack plane. $\theta_p = 0$ represents the crack propagation in the "straight-ahead" direction. θ_p <0 if K_{II} >0, while θ_p >0 if K_{II} <0.

4.6. High strength Line Pipe (HLP) model

As no experimental data is available for validating the developed hybrid fluid-structure model, a simple semi-empirical crack propagation model previously developed based on the pipeline ductile fracture propagation data was used to verify the obtained numerical results. In particular, in order to calculate the crack propagation speed and verify the developed hybrid numerical model the HLP Committee for the ISIJ (Iron and Steel Institute of Japan) method was used. The HLP method is relatively simple algebraic model which is based on the correlation proposed by Makino et al. (Makino et al., 2001). According to this approach the crack speed can be calculated as:

$$\dot{a} = 0.67\frac{\sigma_f}{\sqrt{J_{DWTT}/A_p}}(P/P_a - 1)^{0.393} \tag{28}$$

where P_a is the crack arrest pressure defined as:

$$P_a = 0.382\frac{w_t}{D}\times\sigma_f\times\cos^{-1}\left(exp\left(-\frac{3.81\times10^7[m^3/N]}{\sqrt{Dw_t}}\times\frac{J_{DWTT/A_p}}{\sigma_f^2}\right)\right) \quad (29)$$

In the above equations w_t and D are respectively the pipe wall thickness and the pipe internal diameter in [mm], while A_p is the ligament area of the pre-cracked DWTT specimen in $[mm^2]$, J_{DWTT} is the pre-cracked DWTT energy in [J] and σ_f is the material flow stress in [MPa], which are respectively defined as (Makino et al., 2001; Inoue et al., 2003):

$$A_p = 71.12[mm]w_t \quad (30)$$

$$J_{DWTT} = 3.29w_t^{1.5}J_{CVN}^{0.544} \quad (31)$$

The material flow stress σ_f is defined as:

$$\sigma_f = 0.5(\sigma_y + \sigma_{ult}) \quad (32)$$

where σ_y and σ_{ult} are respectively the yield stress and ultimate tensile stress of the pipeline material.

5. Results and discussion

5.1. DWTT Model validation

In order to validate the developed model, results of the finite element simulation were compared with the experimental data obtained in the DWTT

test (Figure 4). Figure 5(a) shows the comparison of force against hammer displacement and absorbed energy between simulation and experiment. From the figure it can be seen that the simulation slightly overestimates the contact force. However, the estimated results were close enough to the experimental observation. By comparing the amount of absorbed energy, which is the integrated area beneath the force-displacement curve, between the simulation results and the observed experimental data, it can be noticed that the numerical predicted data is in a good agreement with the measured data. Figure 5(b) depicts that as the crack propagates, the maximum stress distribution extends along the loading direction till the middle of the specimen and mode I fracture occurs. Then the mixed mode behaviour governs the failure mode. From the simulation result, it was noticed that, the XFEM-based cohesive segment approach can be a suitable methodology to model brittle fracture behaviour of API X70 pipeline steels. Nevertheless, due to the strong discontinuous behaviour of the XFEM crack propagation process, the possibilities of facing numerical convergence issues are very high.

Figure 6(a) depicts the variation of the calculated dynamic SIF versus δ_{CMOD}. As can be noticed, the relationship between the SIF in dynamic mode is linear with δ_{CMOD}. Figure 6(b) presents the variation of the measured crack propagation speed versus the normalised dynamic SIF calculated using Equation 17. As it is shown in the figure the relationship between the crack propagation speed and the normalised dynamic SIF is logarithmic for the API X70 pipeline steel used in this investigation and can be written as:

$$\dot{a} = C_1 ln\left(\frac{K_{ID}}{\sigma_y\sqrt{a}}\right) + C_2 \tag{33}$$

For API X70 pipeline steel, the DWTT test conditions along with material constants used for simulation are tabulated in Table1.

5.2. Hybrid fluid-structure interaction Model verification

Figure 2 illustrates the three dimensional finite element mesh of the simulated pipe along with the schematic representation of the developed coupling algorithm for modelling running fracture. A pipe section of 10m long, real-scale 48" outer diameter (D) and 18mm thickness was modelled to evaluate the impact of CO_2 fluid phase and pipeline transportation conditions on the rate of brittle fracture propagation. Only half of the pipe section was considered by utilizing the symmetry conditions, as shown in Figure 2. The pipe was fixed at one side and a through-wall starter notch with a length equal to the outer diameter is introduced to trigger crack initiation at the other side. The crack propagation distance was limited to 4 times the outer diameter to reduce the numerical computational time. Isotropic material properties with elasto-plastic behaviour, including damage initiation and evolution laws based on a cohesive segment concept, were defined for the pipe section. 3-D structural 8-node linear brick, reduced integration, hourglass control (C3D8R) elements were used for the pipe section model. The minimum mesh size along the crack propagation path was 6mm and increased gradually far from the area of interest. In order to obtain reliable and robust results from numerical simulations, it is essential to apply the correct loading conditions i.e. internal and back-fill pressure during running fracture in the pipe. In the present study a simplified approach is adapted where effect of back-fill pressure is simulated by an a constant pressure load of 5 MPa is applied on the external surface of the pipe wall as suggested by

Makino et al. (2001).

Figure 7 compares the calculated crack propagation speed of the crack propagation model (XFEM), which is not coupled with the CFD model, the developed hybrid fluid-structure model (XFEM+CFD) and the semi-empirical approach for both upper and lower shelf energies, which is coupled with the CFD model, (HLP+CFD). From these results it can be seen that the XFEM approach without the CFD model and constant pressure over-estimates the crack propagation velocity and the crack speed increases as the crack advances. The main reason for this behaviour is that the ratio between internal pressure and external pressure does not change as the crack propagates, because there is no decompression while brittle fracture is occurring. Comparing the results of XFEM+CFD model with the HLP+CFD approach at lower shelf energy indicates that the estimated numerical results are in good agreement with the calculated semi-empirical solutions.

Figure 8(a) illustrates the running brittle crack in the pipe, the stress distribution at the crack tip and the normalised variation of hoop stress distribution inside the pipe along the crack propagation path. As it is shown in the figure the stress distribution of the pipe can be transformed to cylindrical coordinate system, which results in radial, hoop (circumferential or tangential) and axial (longitudinal) stresses. By definition the hoop stress is a normal stress in the tangential direction (θ), axial stress is a normal stress parallel to the axis of cylindrical symmetry (Z) and radial stress is a stress in directions coplanar with but perpendicular to the symmetry axis (r). In case of the pipe model, the hoop stress is the acting stress to open the crack. As it can be seen from the figure, the hoop stress is almost zero

at the fractured part of the pipe and reaches its maximum, around 4.7 times of the yield stress, at the crack tip. The hoop stress decreases down to 0.25 times of yield stress in the pressurised side (i.e. un-fractured section) of the pipeline. Figure 8(b) shows the area which is plastically deformed, which is also called the process zone, at the crack tip. It should be noted that the crack tip plasticity fulfils the assumption of small scale yielding concept which is necessary for propagating brittle fracture. Figure 8(c) indicates the variation of normalised hoop stress versus the normalised pipeline length for different crack lengths. As expected, the hoop stress at the crack tip declines due to decompression as the crack propagates under mode I fracture.

Figures 9(a) to (d) show the deformed shape of the pipe at different time steps. The figures illustrate the displacement contour plot of deformed pipe in x-direction. It can be seen that at the beginning the maximum displacement was slightly higher than t= 1.8ms, the main reason for that is the high pressure of the CO_2 stream. From t= 1.8 to 7.5ms the pipe is opening and the maximum displacement varies from 26mm to 192mm, respectively. This information has been used to monitor the crack mouth opening distance during running fracture.

The internal pressure of pipe was calculated at each time step during running fracture by means of the CFD model. Figure 10 (a) shows the variation of normalised internal pressure by initial internal pressure versus normalised pipe length. From the figure it can be noticed that the internal pressure is maximum at crack tip and varies smoothly far from the crack tip. These variations tend to zero pressure at fractured part and maximum value at un-fractured ligament of pipeline. Moreover, Figure 10(b) shows the

variation of normalised flow area (A/A_f), where A_f= $28m^2$, during pipeline decompression at different crack lengths.

Figure 11(a) and (b) depict the variation of the normalised mode I and II (opening and shearing crack propagation modes) SIFs during crack propagation and decompression steps. The crack front was meshed using three elements through the pipe wall. Therefore, the SIFs can be extracted at four different nodes through the pipe wall's thickness. As shown in Figure 11(a) these four nodes are named as n1 to n4, in which n1 is the node at outer surface and n4 is the inner surface. From the figure it can be seen that by advancing the crack the mode I SIF (K_I) is decreasing, which clearly results from pipe decompression. This drop is severe at the beginning of the pipe's decompression up to a crack length equal to 0.4 times the pipe length and reaches a plateau from 0.4 till 0.8 times the pipe length, following a tendency to drop at the end of the pipe's section. In addition, it can be seen that the obtained mode I SIFs (K_I) at all points through the pipe's thickness follow a same trend. Nevertheless, the stress intensity is slightly higher inside the pipe, which can be because of the compressive back-fill pressure applied at outer surface of the pipe.

Figure 11(b) shows the variation of the normalised mode II SIF (K_{II}) versus the normalised crack propagation length. The obtained results reveal that the tendency of mixed mode crack propagation is very low. In addition it can be noted that the variation of K_{II} is not the same for the outside and the inside of the pipe. The mode II SIF inside the pipe has almost the same trend as mode I SIF, as shown in Figure 11(a), but outside of the pipe the variation of K_{II} is negligible. Nonetheless, in order to understand

more about the mixed mode behaviour during running brittle fracture, the crack propagation angle was calculated using the maximum tangential stress criterion at each step of crack advancing.

Figure 12 (a) shows the variation the normalised δ_{CMOD} versus normalised crack length during running brittle fracture. As can be seen from the figure, it is possible to model the variation of δ_{CMOD} by means of an exponential function. Moreover, it can be noticed that for a crack length of 5m, the maximum value of normalised δ_{CMOD} is less than 0.4 times of pipe diameter, which proves that, as expected, in case of brittle fracture the pipe opening is not significant. Figure 12 (b) indicates that by increasing the δ_{CMOD} both mode I and II stress intensity factors are declining. These drops are considerable at the beginning of crack propagation and reach a plateau. However, it can be clearly seen that the effect of opening fracture mode (K_I) is more dominant than shear fracture mode (K_{II}).

Figure 13(a) shows the variation of the normalised K_{II} versus the calculated crack propagation angle (θ_p) extracted at the crack front during running fracture. The crack propagation angle is different inside and outside of the pipe and the propagating crack tends to twist slightly. However, the value of crack propagation angle is changing from -4° to approximately 7° and the results show to be more scattered inside of the pipe compared to outside of the pipe. Mode-mixity behaviour of crack propagation, defined as $\varphi = tan^{-1}(K_{II}/K_I)$, was studied to monitor the variation of mode II compared to mode I SIFs. Figure 13(b) shows a linear relationship between mode-mixity and crack propagation angles for all extracted SIFs at the crack front during propagation of the crack through the pipeline. From these re-

sults it can be concluded that the dominating crack propagation mode is mode I and the effect of mode II crack propagation can be neglected, which was the first assumption in this study.

Eventually, in order to study the reliability of material used for CO_2 pipeline, the crack arrest behaviour of has been investigated. To do so, in general, Battelle Two Curve (BTC) method is commonly applied to evaluate the pipeline propensity to fracture propagation by comparing the pipeline depressurisation velocity on the one hand and the fracture (brittle or ductile) velocity on the other hand. According to BTC method the potential crack arrest is indicated if, for any given pressure level during depressurisation, the fracture velocity is lower than or equal to the depressurisation velocity which can be obtained based on fluid dynamics considerations. In this study the brittle fracture propagation velocity was calculated using hybrid fluid-structure interaction modelling approach. Figure 14 shows the comparison between crack propagation and CO_2 decompression velocities obtained for a pre-combustion CO_2 mixture containing 93.1% of CO2, 3.5% of N2 and 3.4% of H2S. From the figure it can be concluded that around crack tip pressure of 4.5MPa the predicted crack propagation velocity becomes lower than the gas decompression velocity curve, which indicate that the propagating brittle crack may become eventually arrested

6. Conclusion

In this study, a hybrid fluid-structure interaction modelling approach has been introduced to simulate brittle fracture propagation in a CO_2 pipeline steel. Using the developed model it was possible to couple the fluid dynamics

between the escaping fluid during decompression and the propagating brittle fracture of the deforming pipeline. In terms of pipeline decompression a one-dimensional compressible CFD model was used to simulate the state of the fluid, which assumes the homogeneous equilibrium nature of the flow. In terms of modelling brittle fracture, the crack propagation was modelled for the instantaneous state of stress as predicted by the CFD model. To do so a novel approach of the eXtended Finite Element Method (XFEM)-based cohesive segment technique was used to model dynamic brittle fracture behaviour of pipeline steel, in which the dynamic SIF and crack velocity were calculated at the crack tip at each step of crack propagation. The proposed model was verified by comparing the obtained numerical results against the available semi-empirical approach from literature. The simulated results were in good agreement with the calculated semi-empirical solutions and indicates the capability of the proposed approach to predict running brittle fracture in a CO_2 pipeline. The results of simulation of a hypothetical but realistic CO_2 pipeline rupture scenario showed that in case of initiation of a brittle fracture it can propagate very fast over a short section of an API X70 pipeline steel transporting CO_2 streams. For future work the proposed model can be used to study the effects of different impurities on brittle fracture behaviour of pipeline steel transporting impure CO_2 streams.

Acknowledgment

The authors gratefully acknowledge the financial support provided by the European Union 7th Framework Programme FP7-ENERGY-2012-1-2STAGE under grant agreement number 309102. The paper reflects only the authors

views and the European Union is not liable for any use that may be made of the information contained therein.

References

Andrews, R., Haswell, J., and Cooper, R. (2010). Will fractures propagate in a leaking CO_2 pipeline? *Journal of Pipeline Engineering*, 9(4).

Aursand, E., Dørum, C., Hammer, M., Morin, A., Munkejord, S. T., and Nordhagen, H. O. (2014). CO_2 pipeline integrity: Comparison of a coupled fluid-structure model and uncoupled two-curve methods. *Energy Procedia*, 51:382–391.

Barsom, J. M. and Rolfe, S. (1970). Correlations between K_{IC} and Charpy V-notch test results in the transition-temperature range. In *Impact testing of metals*. ASTM International.

Belytschko, T. and Black, T. (1999). Elastic crack growth in finite elements with minimal remeshing. *International journal for numerical methods in engineering*, 45(5):601–620.

Billingham, J., Sharp, J., Spurrier, J., and Kilgallon, P. (2003). Review of the performance of high strength steels used offshore. *Health Saf. Exec*, 111.

Brown, S., Martynov, S., and Mahgerefteh, H. (2015). Simulation of two-phase flow through ducts with discontinuous cross-section. *Computers & Fluids*, 120:46–56.

Chen, N. H. (1979). An explicit equation for friction factor in pipe. *Industrial & Engineering Chemistry Fundamentals*, 18(3):296–297.

Corten, H. (1980). A mixed-mode crack analysis of isotropic solids using conservation laws of elasticity. *Urbana*, 3:61801.

Cosham, A., Koers, R., Andrews, R., and Schmidt, T. (2015). Progress towards the new EPRG recommendation for crack arrest toughness for high strength line pipe steels. In *20th JTM*.

Diamantonis, N. I., Boulougouris, G. C., Mansoor, E., Tsangaris, D. M., and Economou, I. G. (2013). Evaluation of cubic, SAFT, and PC-SAFT equations of state for the vapor–liquid equilibrium modeling of CO_2 mixtures with other gases. *Industrial & Engineering Chemistry Research*, 52(10):3933–3942.

Diamantonis, N. I. and Economou, I. G. (2011). Evaluation of statistical associating fluid theory (SAFT) and perturbed chain-SAFT equations of state for the calculation of thermodynamic derivative properties of fluids related to carbon capture and sequestration. *Energy & Fuels*, 25(7):3334–3343.

Dooley, J. J., Dahowski, R. T., and Davidson, C. L. (2009). Comparing existing pipeline networks with the potential scale of future U.S. CO_2 pipeline networks. *Energy Procedia*, 1(1):1595–1602.

Greenshields, C., Venizelos, G., and Ivankovic, A. (2000). A fluid–structure model for fast brittle fracture in plastic pipes. *Journal of fluids and structures*, 14(2):221–234.

Guinea, G., Pastor, J., Planas, J., and Elices, M. (1998). Stress intensity

factor, compliance and CMOD for a general three-point-bend beam. *International Journal of Fracture*, 89(2):103–116.

Higuchi, R., Makino, H., Matsumara, M., Nagase, M., and Takeuchi, I. (2008). Development of a new prediction model of fracture propagation and arrest. In *In: High pressure gas transmission pipeline, 8th International welding symposium, Kyoto, Japan.*

Inoue, T., Makino, H., Endo, S., Kubo, T., Matsumoto, T., et al. (2003). Simulation method for shear fracture propagation in natural gas transmission pipelines. In *The Thirteenth International Offshore and Polar Engineering Conference*. International Society of Offshore and Polar Engineers.

LeVeque, R. J. (2002). *Finite volume methods for hyperbolic problems*, volume 31. Cambridge university press.

Li, S., Thouless, M., Waas, A., Schroeder, J., and Zavattieri, P. (2005). Use of a cohesive-zone model to analyze the fracture of a fiber-reinforced polymer–matrix composite. *Composites Science and Technology*, 65(3):537–549.

Mahgerefteh, H., Brown, S., and Denton, G. (2012). Modelling the impact of stream impurities on ductile fractures in CO_2 pipelines. *Chemical engineering science*, 74:200–210.

Mahgerefteh, H., Oke, A. O., and Rykov, Y. (2006). Efficient numerical solution for highly transient flows. *Chemical engineering science*, 61(15):5049–5056.

Makino, H., Kubo, T., Shiwaku, T., Endo, S., Inoue, T., Kawaguchi, Y., Matsumoto, Y., and Machida, S. (2001). Prediction for crack propagation

and arrest of shear fracture in ultra-high pressure natural gas pipelines. *ISIJ international*, 41(4):381–388.

Maxey, W., Kiefner, J., Eiber, R., and Duffy, A. (1972). Ductile fracture initiation, propagation, and arrest in cylindrical vessels. In *Fracture Toughness: Part II*. ASTM International.

Metz, B., Davidson, O., De Coninck, H., Loos, M., Meyer, L., et al. (2005). *Carbon dioxide capture and storage*. Cambridge university press.

Nishioka, T. and Atluri, S. (1982). A method for determining dynamic stress intensity factors from COD measurement at the notch mouth in dynamic tear testing. *Engineering Fracture Mechanics*, 16(3):333–339.

Nonn, A., Wessel, W., Schmidt, T., et al. (2013). Application of finite element analyses for assessment of fracture bhavior of modern high toughness seamless pipeline steels. In *The Twenty-third International Offshore and Polar Engineering Conference*. International Society of Offshore and Polar Engineers.

Nordhagen, H., Kragset, S., Berstad, T., Morin, A., Dørum, C., and Munkejord, S. (2012). A new coupled fluid–structure modeling methodology for running ductile fracture. *Computers & Structures*, 94:13–21.

O'Donoghue, P., Green, S., Kanninen, M., and Bowles, P. (1991). The development of a fluid/structure interaction model for flawed fluid containment boundaries with applications to gas transmission and distribution piping. *Computers & Structures*, 38(5):501–513.

O'Donoghue, P., Kanninen, M., Leung, C., Demofonti, G., and Venzi, S. (1997). The development and validation of a dynamic fracture propagation model for gas transmission pipelines. *International Journal of Pressure Vessels and Piping*, 70(1):11–25.

Porter, R. T., Fairweather, M., Pourkashanian, M., and Woolley, R. M. (2015). The range and level of impurities in CO_2 streams from different carbon capture sources. *International Journal of Greenhouse Gas Control*, 36:161–174.

Sainte Catherine, C., Hourdequin, N., Galon, P., and Forget, P. (2013). Finite element simulations of Charpy-V and sub-size Charpy tests for a low alloy RPV ferritic steel. In *ECF13, San Sebastian 2000*.

Scheider, I. (2009). Derivation of separation laws for cohesive models in the course of ductile fracture. *Engineering Fracture Mechanics*, 76(10):1450–1459.

Scheider, I., Nonn, A., Völling, A., Mondry, A., and Kalwa, C. (2014). A damage mechanics based evaluation of dynamic fracture resistance in gas pipelines. *Procedia Materials Science*, 3:1956–1964.

Sih, G. C., Paris, P., and Irwin, G. R. (1965). On cracks in rectilinearly anisotropic bodies. *International Journal of Fracture Mechanics*, 1(3):189–203.

Sugie, E., Matsuoka, M., Akiyama, T., Mimura, H., and Kawaguchi, Y. (1982). A study of shear crack propagation in gas-pressurized pipelines. *Journal of Pressure Vessel Technology*, 104(4):338–343.

Talemi, R. H. (2016). Numerical simulation of dynamic brittle fracture of pipeline steel subjected to DWTT using XFEM-based cohesive segment technique. *Fracture and Structural Integrity*, (36):151–159.

Talemi, R. H., Cooreman, S., and Van Hoecke, D. (2016). Finite element simulation of dynamic brittle fracture in pipeline steel: A XFEM-based cohesive zone approach. *Proceedings of the Institution of Mechanical Engineers, Part L: Journal of Materials Design and Applications*, page 1464420715627379.

Thompson, K. W. (1987). Time dependent boundary conditions for hyperbolic systems. *Journal of computational physics*, 68(1):1–24.

Wu, Y., Yu, H., Lu, C., Tieu, A. K., Godbole, A., and Michal, G. (2013). Transition of ductile and brittle fracture during DWTT by FEM. In *Proceedings of 13th international Conference on Fracture, ICF13*.

Yang, X., Zhuang, Z., You, X., Feng, Y., Huo, C., and Zhuang, C. (2008). Dynamic fracture study by an experiment/simulation method for rich gas transmission X80 steel pipelines. *Engineering Fracture Mechanics*, 75(18):5018–5028.

Zucrow, M. J. and Hoffman, J. D. (1976). Gas dynamics. *New York: Wiley, 1976*, 1.

Figures

Fig 1. Dimensions of DWTT specimen with 19mm thickness and the impact loading conditions.

Fig 2. Three dimensional finite element mesh of simulated pipe section along with the schematic representation of the developed coupling algorithm for modelling running brittle fracture and pipeline decompression.

Fig 3. (a) Schematic representation of the pipeline section with a fracture along its length and (b) the corresponding variation in the effective cross-sectional area of the pipeline in the proposed fracture dynamics model.

Fig 4. Two dimensional finite element mesh along with boundary and loading conditions of DWTT, which was used to validate the brittle fracture model and calculate the dynamic SIF at crack tip during running fracture.

Fig 5. (a) Comparison of force against displacement of hammer and absorbed energy between simulation result and experimental observation and (b) contour plot of maximum principle stress (MaxP) distribution during the crack propagation steps for DWTT.

Fig 6. Variation of (a) calculated dynamic SIF versus crack mouth opening distance and (b) calculated crack propagation velocity versus normalised dynamic SIF obtained from DWTT.

Fig 7. Compares the calculated crack propagation speed of crack propagation model, which is not coupled with CFD model, (XFEM), the developed hybrid fluid-structure model (XFEM+CFD) and the semi-empirical approach for both upper and lower shelf energies, which was coupled with FCD model, (HLP+CFD). The crack propagation speed and length are normalised by speed of sound in air (c= 434 $[m/s]$) and pipe length, respectively.

Fig 8. Shows (a) the running brittle crack in the pipe, the stress distribution at crack tip and the normalised variation of axial stress distribution, (b) the plastic stress distribution, which is also call as process zone, at crack tip and (c) the variation of normalised opening stresses versus the normalised pipeline length for different crack lengths.

Fig 9. Contour plot distribution of displacement in x-direction at different crack propagation time steps.

Fig 10. Shows (a) variation of normalised internal pressure by initial internal pressure versus normalised pipe length and (b) normalised flow area (A/A_f), where ($A_f = 28m^2$), during pipeline decompression, which were used as an input pressure in each crack propagation step.

Fig 11. Variation of normalised mode I and II (opening and shearing crack propagation modes) SIFs versus normalised crack length during crack propagation and pipeline decompression.

Fig 12. Shows the variation of (a) normalised crack mouth opening distance versus normalised crack length and (b) normalised mode I and mode II SIFs versus normalised crack mouth opening distance.

Fig 13. Represents (a) the variation of normalised K_{II} versus the calculated crack propagation angle and (b) a linear relationship between mode-mixity and crack propagation angles for all extracted SIFs at crack front during advancing the crack through pipeline.

Fig 14. Shows a comparison between the variation of gas pressure versus decompression velocity for CO_2 and the predicted crack velocity during decompression by means of hybrid fluid-structure interaction modelling approach.

Table 1: DWTT test conditions and material parameters used for simulation

Impact velocity	T	σ_y	T_{max}	Γ	C_1	C_2
6.5[m/s]	-100[°C]	760[MPa]	$1.4\sigma_y$[MPa]	25[MPa.m$^{0.5}$]	324	790

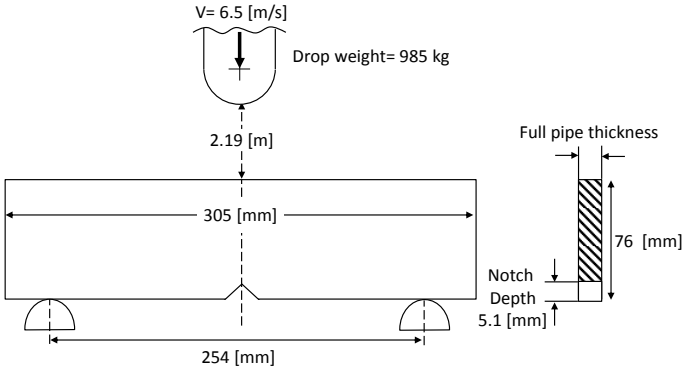

Figure 1: Dimensions of DWTT specimen with 19mm thickness and the impact loading conditions. (Width=9cm)

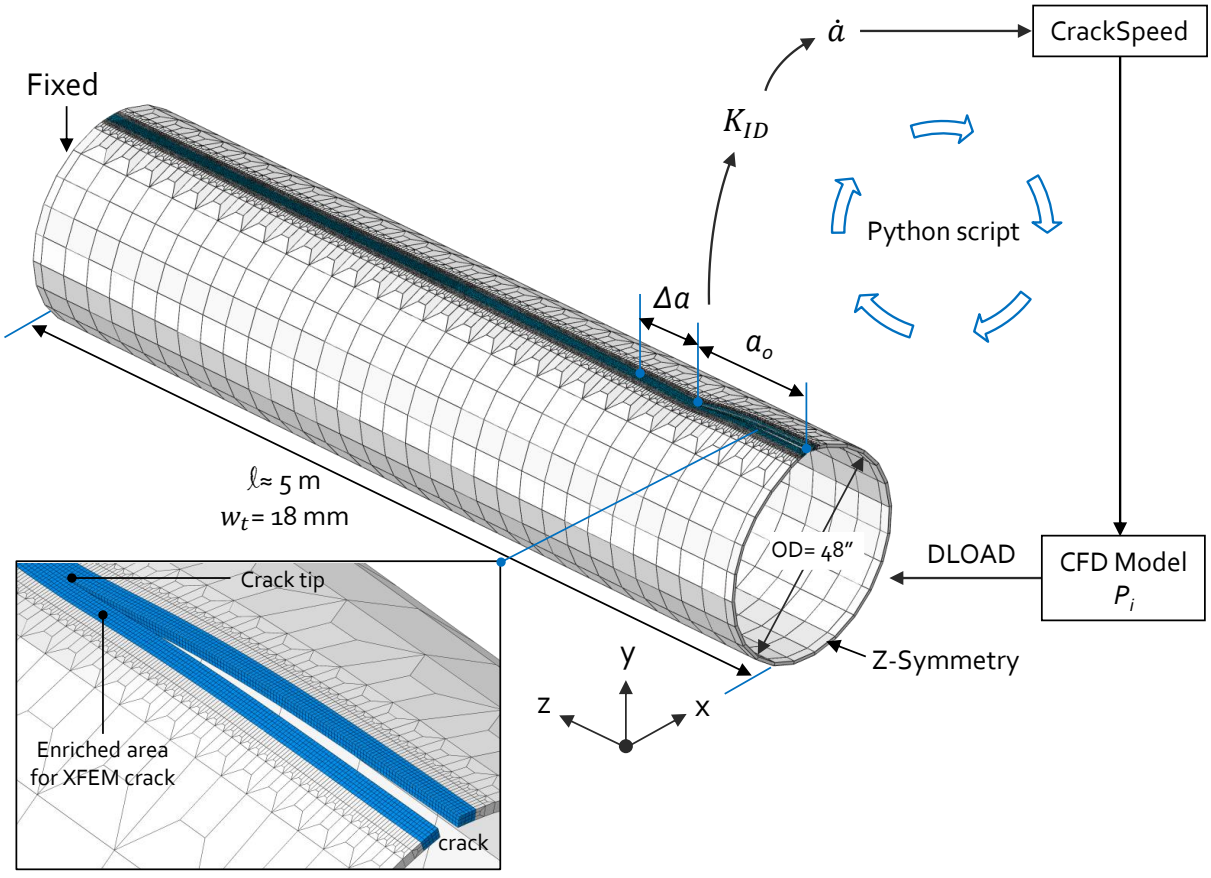

Figure 2: Three dimensional finite element mesh of simulated pipe section along with the schematic representation of the developed coupling algorithm for modelling running brittle fracture and pipeline decompression.(Width=16cm)

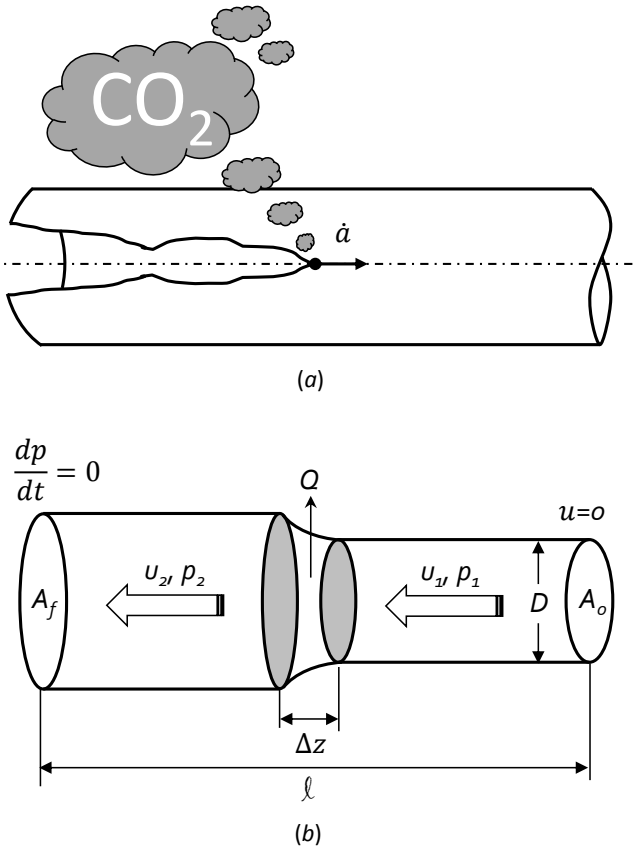

Figure 3: (a) Schematic representation of the pipeline section with a fracture along its length and (b) the corresponding variation in the effective cross-sectional area of the pipeline in the proposed fracture dynamics model. (Width=9cm)

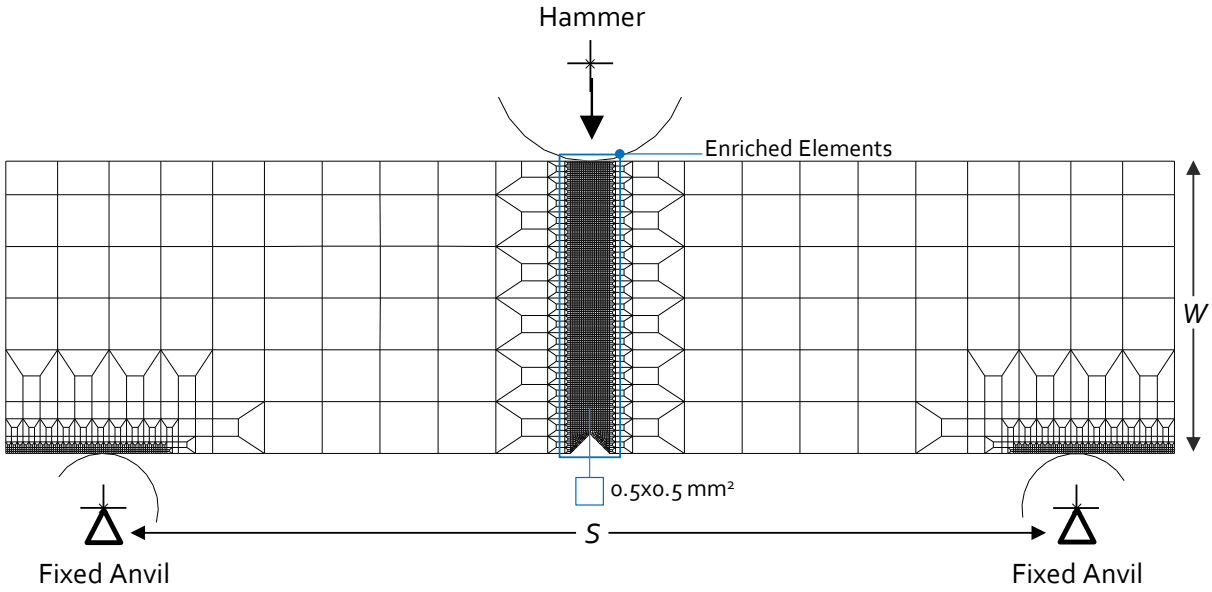

Figure 4: Two dimensional finite element mesh along with boundary and loading conditions of DWTT, which was used to validate the brittle fracture model and calculate the dynamic SIF at crack tip during running fracture. (Width=16cm)

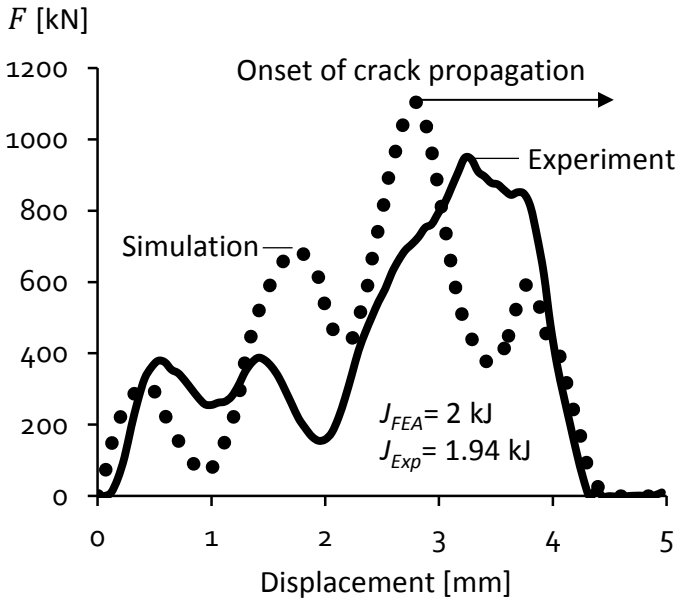

(a)

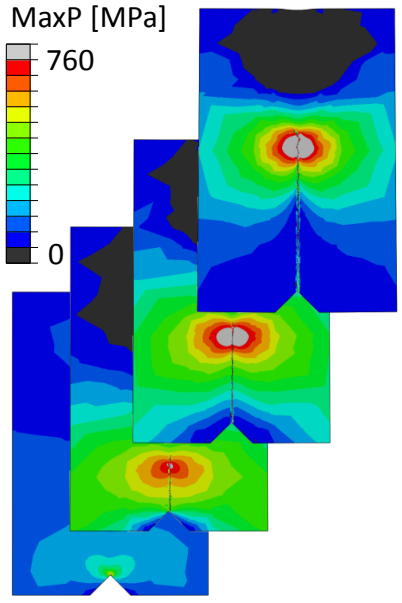

(b)

Figure 5: (a) Comparison of force against displacement of hammer and absorbed energy between simulation result and experimental observation and (b) contour plot of maximum principle stress (MaxP) distribution during the crack propagation steps for DWTT. (Width=9cm)

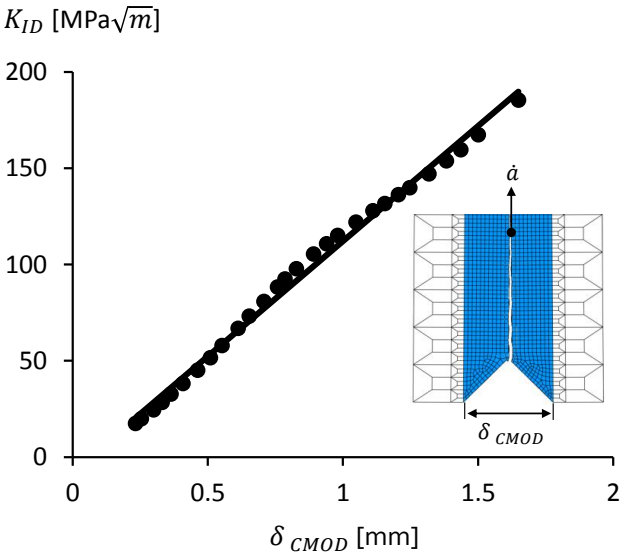

(a)

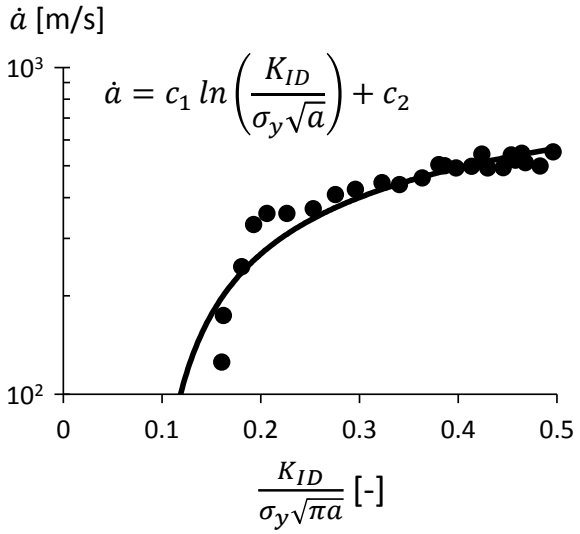

(b)

Figure 6: Variation of (a) calculated dynamic SIF versus crack mouth opening distance and (b) calculated crack propagation velocity versus normalised dynamic SIF obtained from DWTT. (Width=9cm)

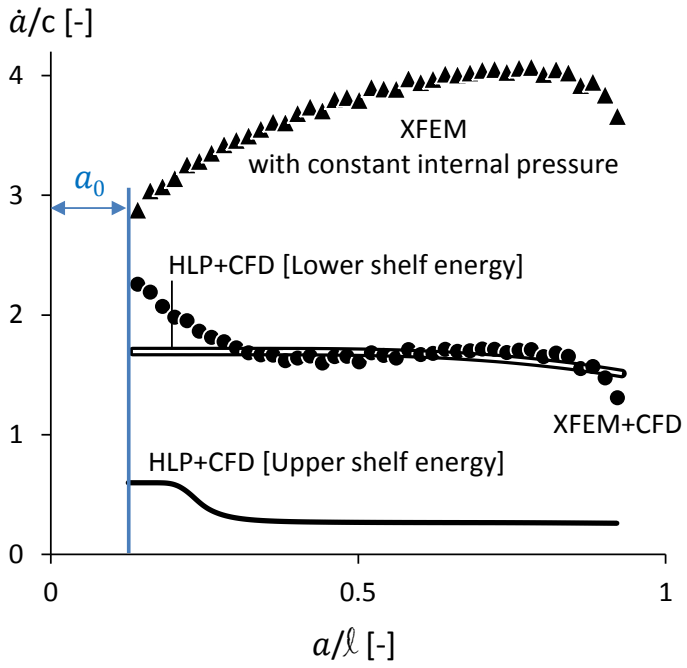

Figure 7: Compares the calculated crack propagation speed of crack propagation model, which is not coupled with CFD model, (XFEM), the developed hybrid fluid-structure model (XFEM+CFD) and the semi-empirical approach for both upper and lower shelf energies, which was coupled with FCD model, (HLP+CFD). The crack propagation speed and length are normalised by speed of sound in air (c= 434 $[m/s]$) and pipe length, respectively. (Width=9cm)

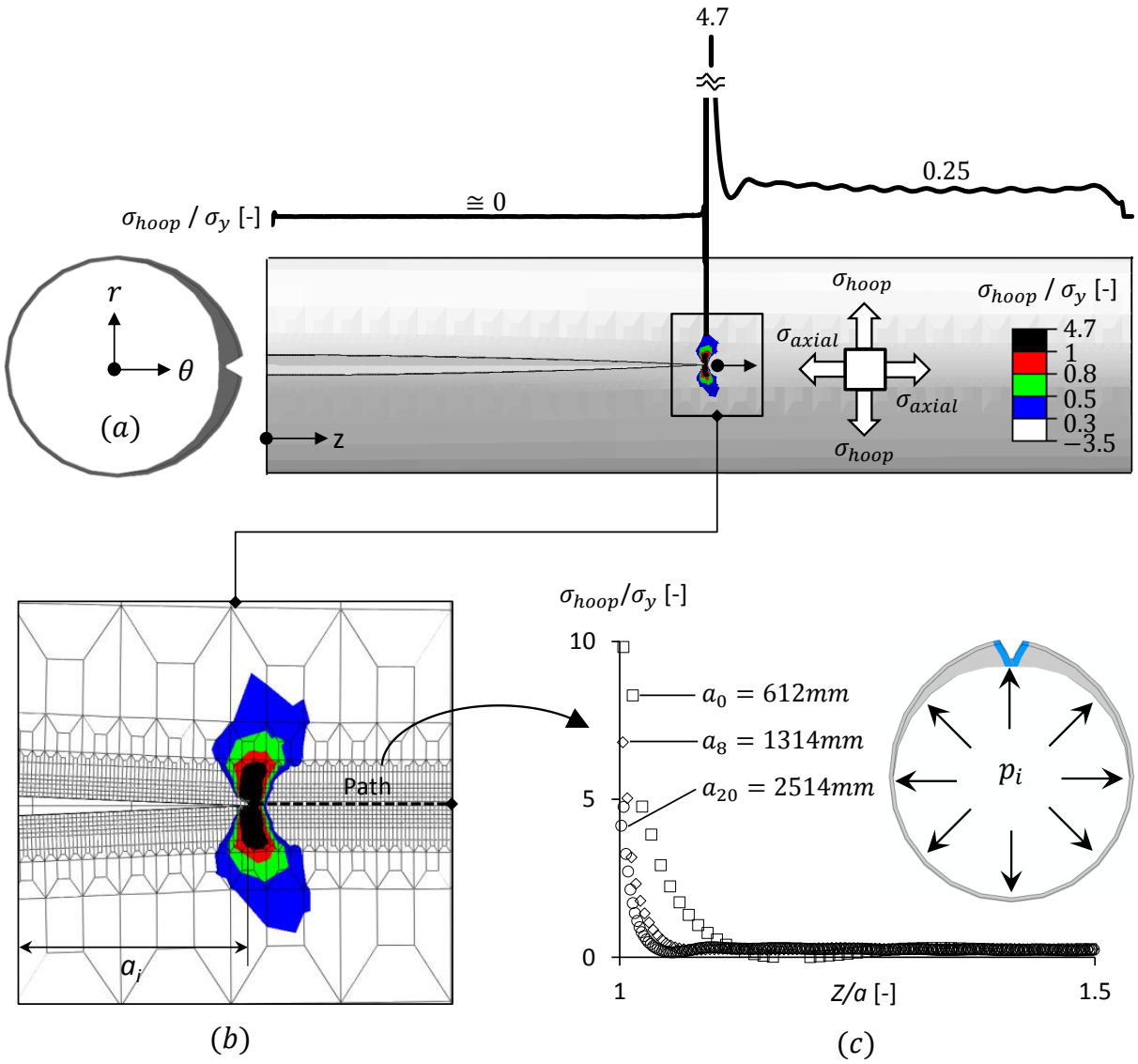

Figure 8: Shows (a) the running brittle crack in the pipe, the stress distribution at crack tip and the normalised variation of axial stress distribution, (b) the plastic stress distribution, which is also call as process zone, at crack tip and (c) the variation of normalised opening stresses versus the normalised pipeline length for different crack lengths. (Width=16cm)

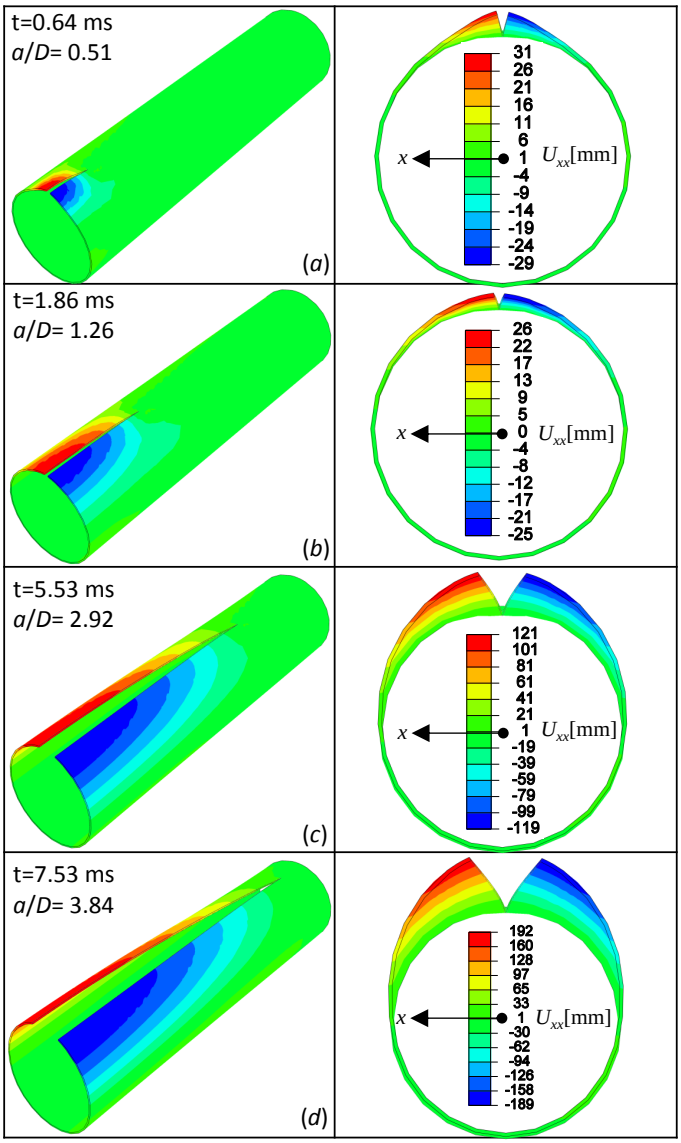

Figure 9: Contour plot distribution of displacement in x-direction at different crack propagation time steps. (Width=9cm)

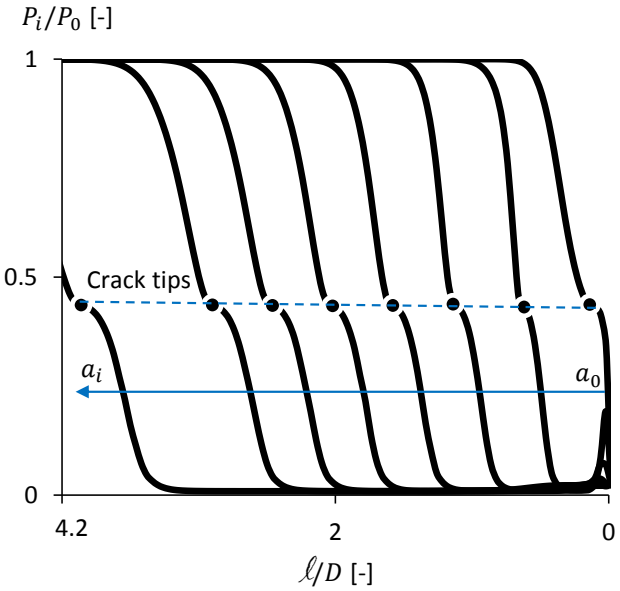

(a)

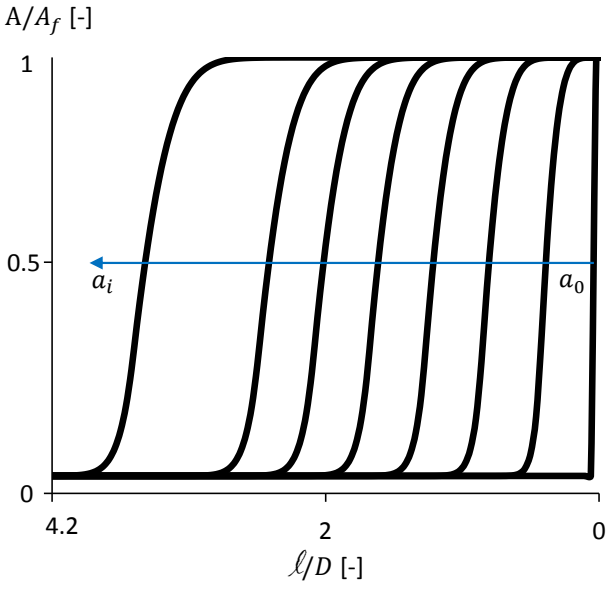

(b)

Figure 10: Shows (a) variation of normalised internal pressure by initial internal pressure versus normalised pipe length and (b) normalised flow area (A/A_f), where ($A_f = 28m^2$), during pipeline decompression, which were used as an input pressure in each crack propagation step. (Width=9cm)

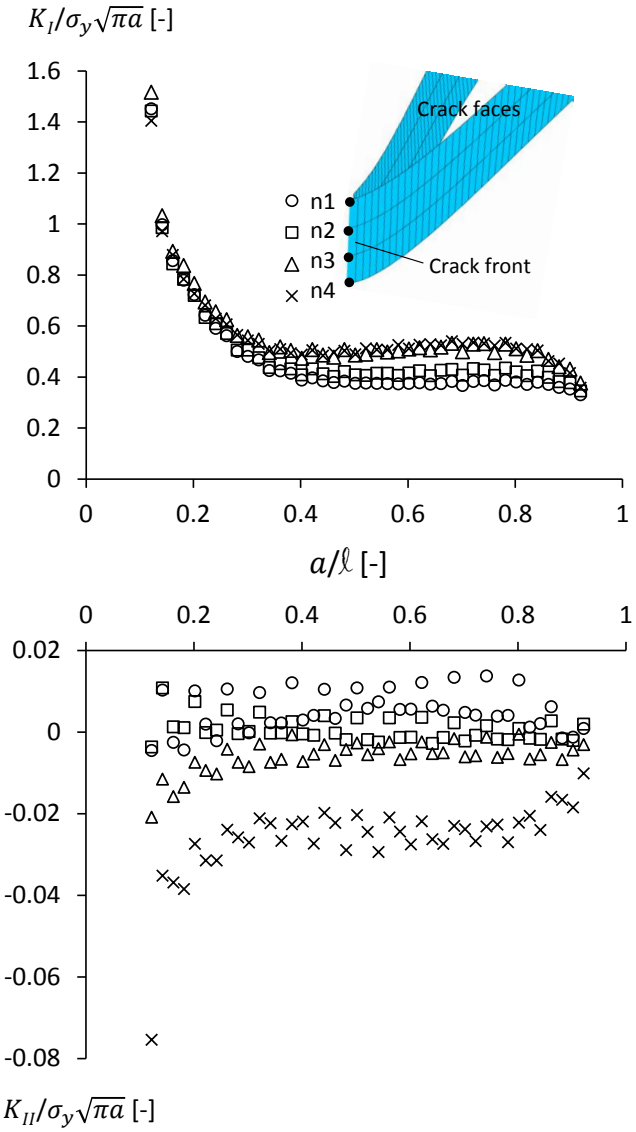

Figure 11: Variation of normalised mode I and II (opening and shearing crack propagation modes) SIFs versus normalised crack length during crack propagation and pipeline decompression. (Width=9cm)

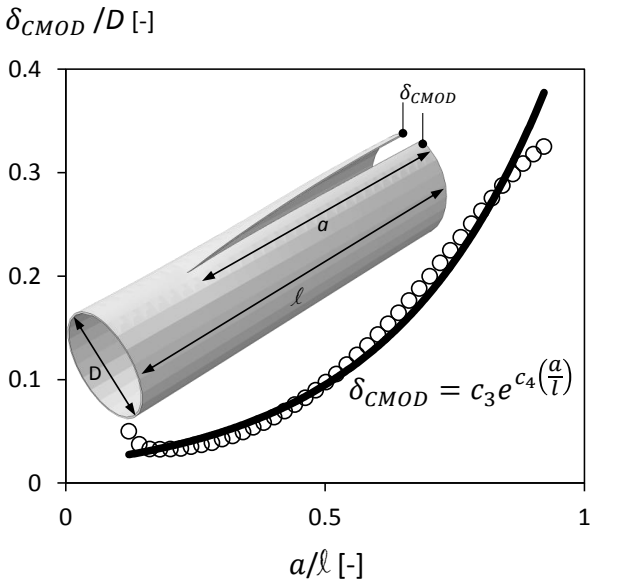

(a)

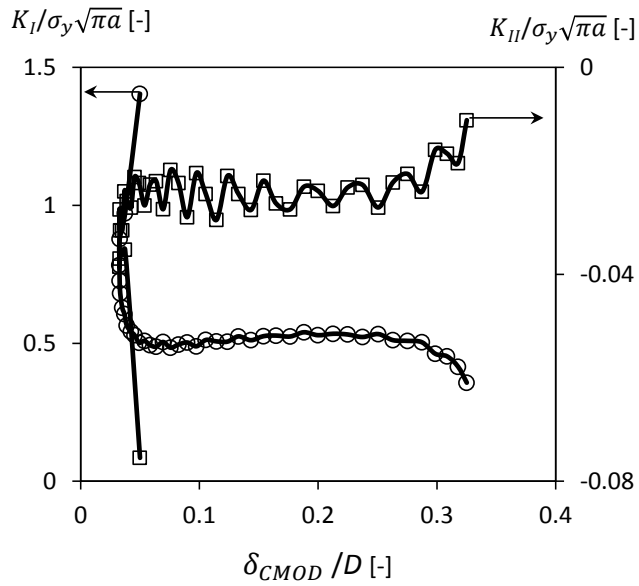

(b)

Figure 12: Shows the variation of (a) normalised crack mouth opening distance versus normalised crack length and (b) normalised mode I and mode II SIFs versus normalised crack mouth opening distance. (Width=9cm)

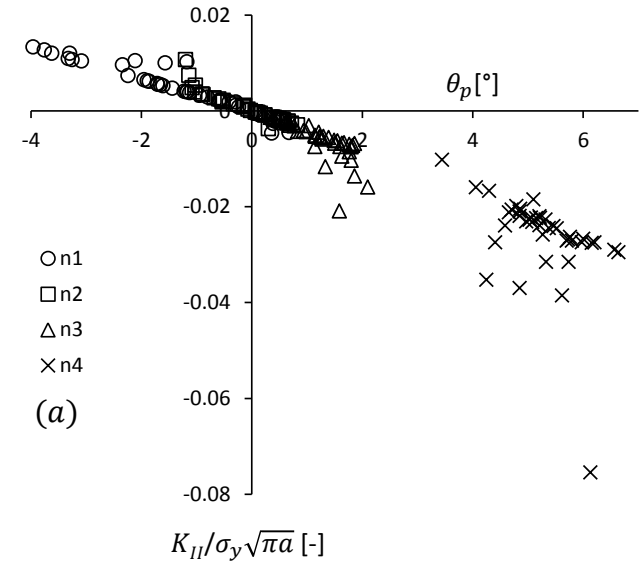

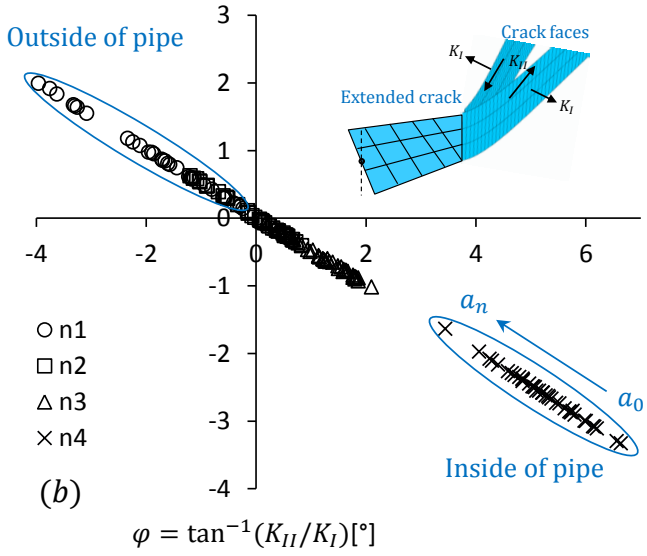

Figure 13: Represents (a) the variation of normalised K_{II} versus the calculated crack propagation angle and (b) a linear relationship between mode-mixity and crack propagation angles for all extracted SIFs at crack front during advancing the crack through pipeline. (Width=9cm)

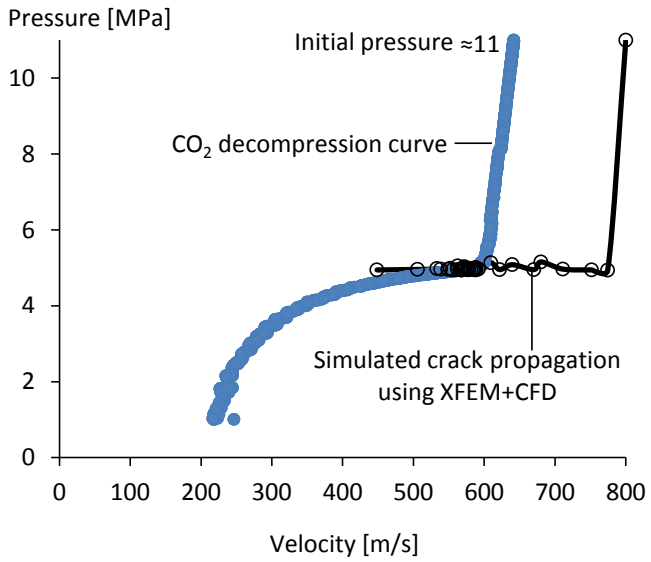

Figure 14: Shows a comparison between the variation of gas pressure versus decompression velocity for CO_2 and the predicted crack velocity during decompression by means of hybrid fluid-structure interaction modelling approach. (Width=9cm)